Accepted by *The Astrophysical Journal*

The Thermal Structure of Gas in Pre-Stellar Cores: A Case Study of Barnard 68

Edwin A. Bergin[1], Sébastien Maret[1], Floris F.S. van der Tak[2], João Alves[3], Sean M. Carmody[4], Charles J. Lada[5]

ABSTRACT

We present a direct comparison of a chemical/physical model to multitransitional observations of $C^{18}O$ and ^{13}CO towards the Barnard 68 pre-stellar core. These observations provide a sensitive test for models of low UV field photodissociation regions and offer the best constraint on the gas temperature of a pre-stellar core. We find that the gas temperature of this object is surprisingly low ($\sim 7-8$ K), and significantly below the dust temperature, in the outer layers ($A_V < 5$ mag) that are traced by $C^{18}O$ and ^{13}CO emission. As shown previously, the inner layers ($A_V > 5$ mag) exhibit significant freeze-out of CO onto grain surfaces. Because the dust and gas are not fully coupled, depletion of key coolants in the densest layers raises the core (gas) temperature, but only by ~ 1 K. The gas temperature in layers not traced by $C^{18}O$ and ^{13}CO emission can be probed by NH_3 emission, with a previously estimated temperature of $\sim 10-11$ K. To reach these temperatures in the inner core requires an order of magnitude reduction in the gas to dust coupling rate. This potentially argues for a lack of small grains in the densest gas, presumably due to grain coagulation.

Subject headings: ISM: Lines and Bands, ISM: Molecules, astrochemistry, ISM:individual (Barnard 68)

[1]University of Michigan, 825 Dennison Building, 500 Church St, Ann Arbor, MI 48109-1042; email: ebergin@umich.edu

[2] Max-Planck-Institut für Radioastronomie, Auf dem Hügel 69, 53121 Bonn, Germany

[3] European Southern Observatory, Karl-Schwarzschild-Strasse 2, 85748 Garching, Germany

[4] 4824 S. 1st Street Kalamazoo, MI 49009

[5] Harvard-Smithsonian Center for Astrophysics, 60 Garden Street, Cambridge, MA 02138

1. Introduction

Several phases of the star formation process have been observationally identified and characterized, beginning with a centrally concentrated core of molecular gas that collapses to form a star surrounded by a disk. Indeed, it has been the isolation of objects that have not yet formed stars – pre-stellar cores – which has allowed us to probe the earliest stages of star formation (see André et al. 2000; Alves et al. 2001; Lee et al. 2001). Of particular importance are the density and temperature structure as these parameters are fundamental to estimating the mechanisms via which cores are supported against gravitational collapse. Moreover knowledge of the physical parameters is a pre-requisite for subsequent chemical and kinematical studies (e.g. van der Tak et al. 2005).

Estimates of the density profile of pre-stellar cores have become quite commonplace through observations of dust emission or absorption. Initial studies have suggested that pre-stellar cores have flat density profiles in the center, falling off as a steep power law in outer layers (e.g. André et al. 2000, and references therein). Less information exists regarding the temperature structure. This is despite the importance of thermal pressure for the stability of pre-stellar cores with little or no turbulent support (Dickman & Clemens 1983; Lada et al. 2003). Initial studies assumed isothermal structure with equivalent gas and dust temperatures (as a result of the anticipated thermal coupling at $n_{H_2} > 10^5$ cm^{-3}; Burke & Hollenbach 1983). More recently, several groups have investigated the thermal structure of dust grains heated by the normal interstellar radiation field (Evans et al. 2001; Zucconi et al. 2001; Bianchi et al. 2003). These studies predict a dust temperature gradient that peaks at 15 – 17 K towards the core edge and declines to near 7 - 8 K at the center in cores with central densities of $\sim 10^6$ cm^{-3}. In this case the actual gas density profile, when estimated via dust continuum emission, could be much steeper than derived assuming constant temperature, for example as steep as r^{-2} (Evans et al. 2001).

Despite the effort placed towards the determination of the dust temperature profile little has been done to characterize the temperature profile of the gas, which is the dominant component. For cores bathed within the average interstellar radiation field (ISRF), theory predicts that the gas temperature will rise towards the cloud edge due to the direct heating of the gas via the photo-electric effect; in shielded gas heating by cosmic rays and dust-gas coupling is expected to dominate (Goldsmith 2001; Galli et al. 2002).

Excellent tracers of the gas temperature are the 22 GHz inversion transitions of NH_3 and cm/mm-wave transitions of H_2CO. Emission from H_2CO has been used to probe the gas temperature in pre-stellar cores by Young et al. (2004) with a finding that this species is heavily depleted in abundance in the center, limiting its value as a probe to outer layers. NH_3 does not appear to exhibit significant gas-phase freeze-out (Tafalla et al. 2002) and

should directly trace T_{gas} deep inside cores. Indeed the gas kinetic temperature derived using ammonia is $\sim 9 - 11$ K, consistent with cosmic ray heating, but above that derived for the dust in similar objects (Tafalla et al. 2002; Hotzel et al. 2002a; Lai et al. 2003; Evans et al. 2001; Zucconi et al. 2001). This is predicted by models of the thermal balance for cores where the central density is $\sim 10^5$ cm^{-3}; in cores with higher densities (e.g. L1544) the gas temperature is expected to drop (Galli et al. 2002). However, NH_3 is limited as a probe of the full thermal structure because its emission does not probe the outer layers of the core seen in other tracers (e.g. $C^{18}O$, CS, H_2CO; Zhou et al. 1989; Tafalla et al. 2002; Young et al. 2004). Thus, while detailed estimates of the dust temperature profile in pre-stellar cores exist and have been compared to observational data, less observational constraints exist for the gas temperature profile.

This paper presents a detailed study of the gas temperature structure in the Barnard 68 pre-stellar core. This well-studied object presents a unique laboratory for study as its density and extinction structure is well determined via near-infrared extinction mapping techniques (see Alves et al. 2001, and references therein). This allows for good constraints to be placed on the line of sight structure in chemical abundance. Observations have shown that this, and other, pre-stellar cores are dominated by selective freeze-out (Tafalla et al. 2002; Bergin et al. 2002), wherein some species (e.g. CS and CO) only trace outer layers and others (N_2H^+, NH_3) trace deeper into the cloud. With knowledge of the chemical structure obtained by detailed models we can determine which tracer is probing a given layer and use multi-molecular studies to reconstruct the physical structure of the cloud. Thus CO and its isotopologues can be used to constrain the gas temperature in the outer low density layers, while NH_3 probes denser gas. This enables us to perform a more detailed examination of the gas temperature structure in the earliest stages of star formation than has been done previously.

In §2 we present our observations and in §3 we discuss the model used to compare to the data. Section 4 compares theory to observations and in §5–6 we discuss the implication of and summarize our results.

2. Observations and Results

The J=1-0 (109.78218 GHz) and J=2-1 (219.560319 GHz) transitions of $C^{18}O$ were observed towards B68 ($\alpha = 17^h22^m38\overset{s}{.}2$ and $\delta = -23°49'34\overset{''}{.}0$; J2000) during April 2000 and 2001 using the IRAM 30m telescope. The entire core was mapped using $12''$ sampling with the half-power beam width of $22''$ at 110 GHz and $11''$ at 220 GHz. System temperatures for the 3mm observations were typically ∼160–190 K with ∼350–450 K at 1mm and integration

times were typically 2–6 min. Pointing was checked frequently with an uncertainty of $\sim 2''$. The data were taken using frequency switching and calibrated using the standard chopper wheel method and are presented here on the T_{mb} scale using standard calibrations from IRAM documentation. For the analysis the $C^{18}O$ J=2-1 observations were convolved to the lower resolution of the J=1-0 transition. The J=2-1 data were reduced by fitting the spectra with Gaussians and in cases where no emission is observed fixing the width and position of the line using a centroid determined from J=1-0 observations. The J=1-0 observations have been published previously by Bergin et al. (2002) and Lada et al. (2003).

Observations of ^{13}CO J=2-1 (220.3987 GHz; $\theta_{MB} \sim 33''$), ^{13}CO J=3-2 (330.588 GHz $\theta_{MB} \sim 22''$), and $C^{18}O$ J=3-2 (329.330 GHz; $\theta_{MB} \sim 32''$) were obtained at the 10.4m Caltech submillimeter Observatory (CSO) during September 7-9, 2003. Data were taken using position switching with an offset of $6'$; larger reference position offsets for the position switched observations were examined with no difference found in the results. Pointing was checked frequently with a typical uncertainty of 3–4″. Typical system temperatures range from ∼400 – 500 K for the J=2-1 transition ($t_{int} \sim 12 - 20$ s) and $\sim 600 - 700$ K ($t_{int} \sim 40$ s) for the J=3-2 transitions. The ^{13}CO transitions were observed over numerous positions in the core with the goal of obtaining data corresponding to a range of total column (as estimated from the extinction map). Observations of $C^{18}O$ J=3-2 were taken towards two positions in the core with relative offsets of $\Delta\alpha = 0$, $\Delta\delta = 0$ and $\Delta\alpha = 24''$, $\Delta\delta = -48''$. No line is detected at either position with a 1σ rms of $\Delta T_A^* = 0.23$ K and 0.25 K, respectively in 0.05 MHz channels. An additional CSO search for $C^{18}O$ J=3-2 emission was performed on May 27, 2005 (by D. Lis) with no emission detected to a level of 0.3 K (1σ) in 0.05 MHz channels.

All data were calibrated to the T_A^* scale using the standard chopper wheel method. To compare the CSO data to IRAM 30m observations we placed the data on the T_{MB} scale. For $C^{18}O$ and ^{13}CO J=3-2 observations of Mars on Sep. 7, 2003 ($\theta_{Mars} = 24.6''$) were compared to a thermal model (M. Gurwell, priv. comm.) to estimate a main beam efficiency of 55%. For J=2-1 we adopt a main beam efficiency of 60% (D. Lis, priv. comm.). To test this cross-telescope calibration we also observed ^{13}CO J=2-1 in Lynds 1544 with the CSO and compared this to similar data obtained with the IRAM 30m (kindly provided by M. Tafalla). We find that the IRAM 30m data (when convolved to the same resolution as CSO) agrees to within 20%. The IRAM data shows stronger emission, which could be attributed to a 10–20% contribution from the error beam of the larger IRAM telescope (see Bensch et al. 2001). Given these differences, we have assigned a calibration uncertainty of 20% to all 230 and 345 GHz data. $C^{18}O$ J=1-0 data are assigned a calibration uncertainty of 10%.

Fig. 1 presents the observational data as a function of visual extinction. In this plot

(and in subsequent plots) the visual extinction was computed for a 24″ beam on the same grid as the molecular observations using the infrared extinction data of Alves et al. (2001). Thus molecular emission is paired with the visual extinction for each position on a point by point basis. Also shown in Fig. 1a is a weighted 1 A_V binned average of the $C^{18}O$ J=2-1/J=1-0 line ratio. This observed ratio shows increased scatter for $A_V < 5$ mag, but the average line lies close to a ratio of ~ 0.9 even at low extinction. Thus, one simple result can be extracted from this data. Because the $C^{18}O$ emission is optically thin the (2–1)/(1–0) emission line ratios can be used to estimate the excitation temperature (which due to the low dipole moment of $C^{18}O$ should be relatively close to the gas kinetic temperature). The (2–1)/(1–0) emission line ratio of ∼0.9 corresponds to an excitation temperature of 7.6 K, in agreement with previous estimates (Hotzel et al. 2002b).

From the ^{13}CO(2-1)/$C^{18}O$(2-1) line ratio of 0.53 we also estimate the $C^{18}O$ J=2–1 emission is nearly optically thick with $\tau \sim 0.8$. Thus, the gas in the region probed by $C^{18}O$ is colder than the canonical 10 K temperature of typically assumed for low mass cores.

3. Model

3.1. Physical Model

The density structure of Barnard 68 has been tightly constrained via near-infrared extinction mapping techniques by Alves et al. (2001) and is consistent with that of a pressure confined self-gravitating isothermal sphere (a Bonnor-Ebert sphere; Bonnor 1956; Ebert 1955). The extinction measurements show a decline from 30 mag to 1 mag within a radial distance of $\sim 120''$ corresponding to ~ 0.067 pc at a our adopted distance of 125 pc (see Fig. 2 in that paper). Thus with a central density of $n_{HI+2H_2} \sim 6 \times 10^5$ cm^{-3}[1], and assuming spherical structure, the density at the core edge is quite high $> 2 \times 10^4$ cm^{-3}. With the sharp fall off characteristic of pressure confined Bonnor-Ebert spheres there is little mass at lower densities. In Fig. 2a we show the adopted density structure as a function of visual extinction, which are the two key parameters used as inputs to the chemical model discussed below.

[1]This central density is derived from the Bonnor-Ebert fit with a value of $\zeta_{max} = 6.9$. The central density, n_c is proportional to $n_c \propto T\zeta_{max}^2/D^2$, where D is the distance and T is the temperature. We have adopted values of n_c from Alves et al. (2001), who assume the gas and dust temperature is 16 K. Based on measurements from NH_3, this temperature is believed to be too high (Hotzel et al. 2002a; Lai et al. 2003). Since the distance is also uncertain we use $n_c = 6 \times 10^5$ cm^{-3}. We have examined models with a density change of $\sim 40\%$ finding no difference in our results.

3.2. Chemical/Thermal Model

The chemical model adopted in this work is the gas-grain network described previously in Bergin et al. (1995) and Bergin & Langer (1997). We have used a smaller chemical network that focuses exclusively on the formation of CO and simple oxygen bearing molecules. This network was used by Bergin et al. (1998) and has been tested against the larger network for consistency. The network includes the effects of molecular freeze-out onto grain surfaces and desorption via cosmic ray impacts (Hasegawa & Herbst 1993; Bringa & Johnson 2004) and ultraviolet photodesorption. The rate of UV photodesorption is given by R = $2 \times 10^{-10} Y G_0 exp(-1.8 A_V)$ molecules^{-1} s^{-1} (Boland & de Jong 1982; Draine & Salpeter 1979), where Y is the yield (probability of ejection from mantle per photon absorbed). We have adopted $Y = 10^{-3}$ in our work.[2]

The reaction network has been expanded to include the effects of isotopic fractionation using the rates and formalism described in Langer et al. (1984) and isotopic selective photodissociation using the self-shielding rates of van Dishoeck & Black (1988). For solving the chemical equations we use the DVODE algorithm (Brown et al. 1989).

The binding energy of molecules to grain surfaces will influence the evaporation rates. In this work we assume a CO binding energy of 1181 K, which is equivalent to CO bound on water ice (Collings et al. 2003).[3] All other binding energies are based upon the work of Hasegawa & Herbst (1993).

To examine the thermal balance we use a variant of the chemical/dynamical model presented by Bergin et al. (2004), which directly linked the time dependent chemistry to the thermal balance. Heating contributors included cosmic rays, X-rays, and the photoelectric effect with cooling arising from atomic fine structure and molecular rotational transitions. References for the adopted formalism are provided in Table 2 of that paper. Some changes are adopted in the present work. We use the formalism for cosmic ray heating from Wolfire et al. (1995) and have included the cooling contribution from ^{13}CO using the tables (for CO) of Neufeld et al. (1995). We have also adopted the gas-dust coupling rate from Tielens & Hollenbach (1985). For the dust temperature we use the analytical expressions from Zucconi et al. (2001), which used the Mathis et al. (1983a), taking into account the latest adjustments from Black (1994). We did account for variation of the dust temperature with

[2]Recent laboratory measurements of CO photodesorption suggest a probability well below our assumed value, with $Y < 1.9 \times 10^{-5}$ (van Broekhuizen 2005). We have examined a model with this yield and find only a small (10–15%) effect on the ^{13}CO and C^{18}O emission.

[3]Note that this value is substantially lower than previous measurements (Sandford & Allamandola 1988).

a lower external UV field by adding additional layers of extinction based upon the following expression: $A_{V,add} = log(G_0)/(-2.5)$. This expression assumes that the heating effects of the UV field decay as $e^{-2.5A_V}$ and is likely an overestimate (to below a factor of $\sim$1.5) as longer wavelength photons also contribute to dust heating. However, it provides a crude estimate of the effects of a variable UV field. The dust temperature is assumed to be constant with time, while the gas temperature will change as the chemistry evolves.

Since B68 is a cold pre-stellar object bathed in the normal interstellar radiation field (ISRF) we have not coupled the thermal balance directly to the chemistry. Rather the chemistry is calculated assuming a constant temperature of 10 K and the thermal balance is determined using the results from the time-dependent chemical model. Both the chemistry and the thermal balance assume the density profile (derived from dust absorption) is constant with time. In this fashion, for each time, we derive chemical abundances as a function of cloud depth and then compute the resulting thermal balance. This separation is reasonable given that the gas-phase chemistry is rather insensitive to the few degree changes as a function of depth that are found from our thermal balance calculations. The primary temperature dependence in the chemistry arises from the isotopic fractionation of CO at the cloud edges, where the column is small. For example, 2–3 K changes in temperature show 20% differences at the peak $C^{18}O$ abundance.

Since we have adopted a density profile that is constant with time we have assumed that the chemistry has previously evolved at lower density to the point that all carbon resides in CO and oxygen is locked on grains in the form of water ice. In Table 1 we provide a list of assumed initial abundances.

The variables in our calculations are (1) the overall intensity of FUV radiation field, parameterized by G_0, the FUV flux relative to that measured for the local ISM by Habing (1968). This influences the photodissociation rate (at what depth a given CO isotopologue appears) and the amount of photoelectric heating, which dominates the heating at low A_V. (2) Several values of the primary cosmic ray ionization rate were examined between $\zeta = 1.5 - 6.0 \times 10^{-17}$ s^{-1}. CO is assumed to be pre-existing in our calculations and changes in the cosmic ray ionization rate by factors of a few does not change its chemistry appreciably, which is dominated by the grain freeze-out. It does however change the cosmic ray heating rate, which is important for gas heating at high extinction. Because the cosmic ray desorption rate is uncertain we assumed a constant rate in our analysis based in the formalism of Hasegawa & Herbst (1993) and the binding energy given above. (3) Time is also a variable. As the chemistry evolves the effects of freeze-out alters the resulting emission. (4) The final variable is dust-gas heating/cooling rate. The dust-gas thermal coupling expression from Tielens & Hollenbach (1985) is given as:

$$\Gamma_{gas-dust} = 3.5 \times 10^{-34} n^2 \delta_d T_{gas}^{0.52} k(T_{dust} - T_{gas}) \text{ ergs cm}^{-3}\text{s}^{-1}.$$

In this expression δ_d is the ratio of the dust abundance in the modeled region to that of the diffuse ISM. Effectively this is a measure of the surface area trapped in more numerous small grains, which are more efficient in thermally coupling to the gas. When δ_d is varied in our models we make no correction for this in the chemistry, where it can alter the timescales. In general, chemical models assume that large grains are responsible for freeze-out (which is the dominant effect in this calculation). This assumes that cosmic rays can effectively thermally cycle small grains and leave the surface bare (Leger et al. 1985). Thus the change in the surface area or number density of the large 1000 Å grains from the loss of small grains is assumed to be small.

Our analysis proceeds in the following fashion. The adopted $n_{H_2}(r)$ profile and $T_{gas} = T_{dust} = 10$ K is used as inputs to the time-dependent gas-grain chemical model. The results from the chemical model are used as inputs to the thermal balance calculation which provides $T_{gas}(r)$. The abundance and gas temperature structure are incorporated as inputs to the one-dimensional spherical Monte-Carlo radiation transfer model (Ashby et al. 2000). This model self-consistently solves for the molecular emission accounting for effects of sub-thermal excitation, radiation trapping, and pumping by dust continuum photons. The latter is unimportant for B68. Additional inputs to this model are the velocity line width and line of sight velocity field. The line width includes contributions from the thermal and turbulent widths. In our iterations we have assumed a static cloud with the turbulent contribution to the linewidth included that increases with radius from the core center (as required by observations; Lada et al. 2003). The model emission is convolved to the observed angular resolution for each transition (assuming a distance of 125 pc) and onto a grid sampled every 12″. The model emission is then placed onto $\int T_{mb} \Delta v$ vs. A_V plots shown in §4. To compare the velocity width to the data we fit spectra with Gaussians. To be successful a model must reproduce both the dependence of $\int T \text{dv}$ with A_V for $C^{18}O$ J=1-0, ^{13}CO J=2-1, J=3-2, the $C^{18}O$ J=2-1/1-0 integrated emission ratio, and Δv with radius for $C^{18}O$ J=1-0 and ^{13}CO J=2-1.

4. Analysis

4.1. Time Dependent Chemistry and Gas Temperature

In our analysis it became clear that we cannot reproduce the observed emission with the core exposed to the standard ISRF ($G_0 = 1$). Instead these data require colder outer layers and a reduced UV field, $G_0 \sim 0.2$. For our initial discussion of the overall gas temperature structure in cores dominated by freeze-out, we use the model with the reduced UV field. In § 4.2 we demonstrate this requirement.

In Figure 2 we provide a 4 panel plot with the relevant physical quantities that are inputs (e.g. density, dust temperature) or outputs (gas temperature, abundance) from the model. To aid the discussion, we also provide the major heating and cooling terms, as a function of cloud depth. In Fig. 1 we provide the results from a series of time-dependent models superposed on the observational data for B68. This series of four panel plots of the $C^{18}O$ J=2-1/J=1-0 integrated emission ratio plotted as a function of A_V (Fig. 1a), along with the integrated intensity of $C^{18}O$ J=1-0 (Fig. 1b), J=3-2 (Fig. 1c), and ^{13}CO J=2-1 (Fig. 1d) as a function of A_V are used to test our models. In each panel the symbols are data points and lines are the model results.

The models shown in Fig. 1 sample a range of times and assume a cosmic ray ionization rate of $\zeta = 3.0 \times 10^{-17}$ s^{-1}, $\delta_d = 1$, $G_0 = 0.2$. Our "best fit" model is at a time of t $\sim 10^5$ yr, with earlier and later times showing significant discrepancies with observed emission. "Best-fit" implies agreement with CO isotopologue data. As discussed later some modifications to this model are needed to match additional observations. The primary effect of time in the models is increasing CO freeze-out, which lowers the column density as the core evolves. Thus, the drop in $C^{18}O$ and ^{13}CO column density directly relates to the reduction in predicted line intensity. The magnitude of the decline depends on the optical depth of the transition, hence it is largest for thinner $C^{18}O$ J=1–0 emission and smaller for thicker ^{13}CO emission lines. The $C^{18}O$ line ratio does not show strong time-dependence because CO freeze-out, and the subsequent decrease in CO cooling, does not produce a sharp temperature rise. This is demonstrated in Fig. 3 where we present the temperature and CO abundance structure as a function of time. As time evolves in regions with lower density gas with weaker gas-dust coupling ($A_V < 10$ mag), the depletion of coolants warms the gas, but the cooling power of dust-gas collisions compensates for this loss in the densest regions ($A_V > 10$ mag), a point first noted by Goldsmith (2001). The CO abundance exhibits a sharp drop below $A_V = 1$ mag due to photodissociation and decline at high A_V due to freeze-out. The CO photodissociation front is confined to a small range of visual extinction because of the high densities and low UV fields at the boundary layer.

Overall, the gas temperature shows structure but remains within a narrow range of 7 – 9 K. The structure is due to the interplay between the rise and fall of varied heating and cooling agents. At very low A_V (below $\sim$ 0.1 mag) the sharp drop of gas temperature is due to the rise of CO as a gas-phase coolant. The gas temperature shows a slight increase at $A_V \sim 0.1$ mag as the cooling power of C^0 and C^+ is lowered as a direct result of CO formation. Between A_V 0.2 to 1.7 mag the temperature declines due to the decreasing efficiency of photoelectric heating. The decline is reversed for $A_V > 1.7$ mag when the sharp density increase, higher dust temperature, and CO freeze-out combine to produce a rise in dust-gas collisional heating with a reduction in cooling power that compensate for the loss of photoelectric heating. We note that the gas temperature is low between $A_V = 1 - 4$ mag precisely because CO is present as a coolant. When $T_d < T_g$ ($A_V \sim 7.5$ mag) dust collisions become gas coolants producing a slow temperature decline towards the core center. In these models the gas and dust are never completely coupled.

4.1.1. Turbulent Velocity Width

Fig. 4 presents the spectral line full width at half-maximum (FWHM) as a function of radial distance from the extinction peak (i.e. the assumed center of gravity). For the data in this plot the velocity FWHM is determined by Gaussian fits to each spectrum with a $\geq 5\sigma$ emission line detection. The variation of $C^{18}O$ J=1-0 linewidth with position has been discussed previously by Lada et al. (2003). However, the ^{13}CO J=2-1 profiles are much wider and exhibit more scatter.

Our best fit model (solid lines) faithfully reproduces the variation in both $C^{18}O$ and ^{13}CO. The linewidth difference between these two species can be interpreted by the ^{13}CO J=2-1 emission becoming optically thick in outer layers with higher velocity dispersion. We estimate $\tau \sim 5$ for ^{13}CO J=2–1 (from the observed $C^{18}O/^{13}CO$ J=2–1 line ratio and $^{12}C/^{13}$=65) and $\tau \sim 0.7$ for $C^{18}O$ J=2–1. With lower opacity $C^{18}O$ emission traces a larger volume dominated by layers with lower turbulence. Thus in comparative chemical studies the variation in the velocity linewidth can contain information on the depth that is being probed.

4.2. Constraints on the External FUV Radiation Field

As noted earlier the model can not match these data assuming a core bathed within the standard interstellar UV radiation field. This is demonstrated in Fig.5 where we present

models with two different values of G_0. We note that other values of G_0 were examined and present here two extremes; only values of $G_0 \lesssim 0.2$ can match our data. The $G_0 = 0.2$ model, which is our best fit solution, matches all data to within the errors. The $G_0 = 0.9$ model fails on two accounts. (1) Enhanced $C^{18}O$ photodissociation lowers the abundance, resulting in an inability, *at any time*, to reproduce the $C^{18}O$ integrated emission. (2) The gas temperature (see Fig. 2a) in the outer layers is warmer, resulting in stronger ^{13}CO emission than observed. An additional demand for a colder cloud is $C^{18}O$ J=3-2 emission, which was not detected on two separate occasions to a level of $T_{MB} \sim$1.2 K (3σ; § 2). Our best-fit model produces an peak intensity for this line of 1.6 K, which along with ^{13}CO J=3–2, may indicate that this model is still too warm. In sum, ^{13}CO data, and $C^{18}O$ line ratios, suggest temperatures that are quite cold, $\lesssim$ 8 K, even in the layers with relatively low extinction ($A_V = 1$ mag). The temperature is below the assumed dust temperature at these depths.

One issue with our model and the predicted strong ^{13}CO emission for $G_0 = 0.9$ is that the velocity field is treated as static. Contributions from the line of sight velocity field to the line profile have been accounted for within the increasing turbulent contribution to the velocity width (§ 3). B68 has clear evidence for rotation which induces line shifts of up to 50% of the linewidth across the face of the cloud. If rotation were included in the model it could potentially lower the opacity of the optically thick ^{13}CO line emission. We have investigated this possibility using the 2-D Monte-Carlo radiation transfer code of Hogerheijde & van der Tak (2000) and the rotation rate of 4.77 km s^{-1} pc^{-1} estimated by Lada et al. (2003). The rotation axis of B68 shows a small 6 degree slant which may be indicative of some tilt along the line of sight. However, since this is small we have assumed the rotation is oriented along the plane of the sky. We find that the effect of rotation on the ^{13}CO emission is small with only a 10% change in the opacity. Thus, rotation cannot be an answer for the weak ^{13}CO emission.

In addition, rotation cannot account for optically thin $C^{18}O$ J=1-0 emission, where the integrated intensity depends strongly on its abundance. Rather, the photodissociation rate (with self-shielding) plays a major role in determining whether enough $C^{18}O$ exists to emit at appreciable levels. Moreover, the non-detection of optically thin $C^{18}O$ J=3-2 emission suggests that the layers traced by these species need to be cold with $T_{gas} < 8$ K.

Another tracer of the external FUV field is optically thick ^{12}CO emission. In B68 the J=1-0 transition has been detected with a line peak intensity of $T_{mb} = 6.7$ K (F. Bensch, priv. comm.; KOSMA). Our $G_0 = 0.9$ model predicts $T_{mb} \sim$8.7 K, while our best fit model predicts $T_{mb} \sim$2.7 K. We note that the external temperature in our best fit model is 16 K, but that this warm gas does not fill significant volume. Given this trend our models clearly rule out an external field as strong as the Draine (1978) UV field ($G_0 = 1.7$) and argue

for something smaller than the Habing (1968) field. This is in agreement with the study by Young et al. (2004) who also found low UV fields are needed to match CO emission in three pre-stellar cores embedded in the Taurus Molecular Cloud, although they also found evidence for high external temperatures of 10 – 14 K.

4.3. Model Sensitivity and Inner Core Gas Temperature

4.3.1. Cosmic Ray Heating

The chemical/thermal model does exhibit moderate sensitivity to the assumed level of cosmic ray heating. In Fig. 6 we provide a comparison of the observations to models with three different values of the cosmic ray ionization rate. Fig. 7 provides the derived temperature structure from each model. Some temperature differences are found for $A_V > 1$ mag, the depth where cosmic ray heating becomes significant when compared to photoelectric heating (Fig. 2). Models with $\zeta \sim 1.5 - 3.0 \times 10^{-17}$ s^{-1} provide reasonable matches to the data. In contrast, when $\zeta > 6.0 \times 10^{-17}$ s^{-1} the gas temperature in depths traced by C^{18}O and ^{13}CO rises to a point where the model/observation comparison is not as favorable. Given the assumed observational errors, our models find reasonable fits with $\zeta = 1 - 6 \times 10^{-17}$ s^{-1}. The derived cosmic-ray ionization rate is consistent with the value estimated by van der Tak & van Dishoeck (2000) and Webber (1998).

4.3.2. Dust-Gas Coupling

Since CO and its isotopologues are heavily depleted in abundance in the central core it is worth examining whether our model sets any constraints on the central core temperature. This is important because observations of NH_3 in B68 suggests gas temperatures ∼10–11 K (Hotzel et al. 2002a; Lai et al. 2003). Ammonia likely forms from N_2H^+ (Aikawa et al. 2005), which itself only forms in abundance when CO freezes onto grains. Thus ammonia is chemically selected to probe the gas in regions where CO is losing sensitivity. This suggests that the temperature deeper in the cloud may be warmer than the $\sim 8 - 9$ K in our best-fit model.

Fig. 8 and Fig. 9 provide the comparison of theory to observations and the temperature profiles for models where we vary δ_d (the ratio of dust abundance in modeled region to that of the diffuse ISM). We find that to reach $T_{gas} \sim 10$ K, in the central core, as inferred from NH_3 emission line ratios, requires an order of magnitude reduction in the dust-gas thermal coupling rate ($\delta_d = 0.1$). This has a small effect on the C^{18}O and ^{13}CO emission

demonstrating that their emission is not a probe of the inner core gas temperature. Curiously lowering the dust-gas thermal coupling rate reduces $C^{18}O$ and ^{13}CO emission. This is because these two species are predominantly tracing depths where collisions with dust are heating the gas (see Fig. 2). Thus, provided our understanding of dust-gas thermal coupling rates is correct, to match NH_3 derived gas temperatures requires a reduction in the rate, potentially due to changing dust properties.

The conclusion regarding weaker gas-dust coupling rests upon proper modeling of the dust temperature and the calibration of the ammonia thermometer. In our models we have not directly examined dust emission and used the formula provided by Zucconi et al. (2001) with some modifications to account for reduced radiation field (§3). Our modifications to the dust temperature did result in reducing the dust temperature at high depth into the cloud. However, at $A_V > 10$ mag our "best-fit" solution assumes $T_{dust} \sim$8 K, which is quite close the value for similar depths used by Galli et al. (2002) in their core stability study of B68 and is also similar to the value inferred by Zucconi et al. (2001) and Evans et al. (2001) for the inner radii of Bonnor-Ebert spheres. Thus our the requirement for reduced dust-gas coupling would not be altered with more exact treatment of the dust emission.

One question is whether the ammonia thermometer and measurements are calibrated to an accuracy of $\sim$ 2 K. The Hotzel et al. (2002a) measurement of the gas temperature from ammonia emission taken with a similar resolution ($40''$) to our data. The raw error of this measurement is 9.7 $\pm$0.3 K, which is increased to 1.0 K allowing for 20% differences in the filling factor and T_{ex} between the two lines. This seems overly generous given the similarity in critical density and filling factor between these lines. Moreover the Lai et al. (2003) temperature estimate is 10.8 $\pm$0.8 K. Thus both analyses suggest at least a 3σ difference between the central core gas temperature in our model of $\sim$ 8 K and measurements. Regarding the calibration of the ammonia thermometer, for T > 10 K the observed (2,2) and (1,1) inversion transition rotational temperature is not equivalent to the gas kinetic temperature. However, close to 10 K the rotational temperature is a measurement of T_k without any correction (Danby et al. 1988). Thus, provided this calibration is accurate, the observed difference is suggestive that the dust-gas coupling needs to be reduced.

Given the need for lower dust-gas thermal coupling in Fig. 10 we re-examine the time evolution of the gas temperature in a model with reduced coupling. Similar to the discussion in § 4.1, we find that as time evolves and gas coolants deplete the gas temperature rises. In this case the effects of freeze-out on T_{gas} are stronger, but at most depletion warms the core by $\sim$ 1 K. The temperature is actually lower between $0 < A_V < 7$ mag, because the main heating mechanism is dust collisions in this region. Thus, while we have found that freeze-out does raise the temperature, these effects are small and we remain in agreement

with previous studies of the gas temperature in cores dominated by freeze-out (Goldsmith 2001; Galli et al. 2002).

5. Discussion

5.1. The Meaning of Time in these Models

In our models we find a "best-fit" to the observations at t $\sim 10^5$ yr. This does not suggest that we constrain the age of this object to be 10^5 yrs. We have used a density profile that is fixed in time in our time-dependent chemical calculations. Thus we have not accounted for contemporaneous density evolution along with the chemistry. To compensate for this effect we have assumed that all CO is pre-existing in the gas at t = 0 in our chemical network solutions. With these assumptions this time is not the time since the cloud became molecular (since CO is pre-existing) nor is the time since the density structure evolved (since the structure is fixed). Rather, the best-fit time represents the time where sufficient pre-existing CO has been frozen onto grains and the predicted gas emission matches observations. We have also assumed a sticking coefficient of unity. A lower value would result in a higher age determination. Moreover, if we had included any the effect of dust coagulation on the chemistry there would be an increase in the derived timescale. In this sense our derived time is only a *lower limit* to the true age of B68.

We have included a mechanism for returning CO to the gas via constant cosmic ray desorption of CO ice, which does depend on our assumed binding energy. In our models we do not reach a time where desorption is relevant in the sense that at late times when pre-existing CO is frozen and equilibrium is reached between desorption and depletion there is not enough CO in the gas to reproduce the observed emission. The binding energy would need to be lowered well below measured values (Collings et al. 2003) and the rate of CO desorption increased above estimated levels (Bringa & Johnson 2004) to change this condition and raise our time estimate.

5.2. Grain Evolution

Our multi-molecular comparative chemical study (e.g. CO and NH_3) suggests that the dust-gas coupling rate is reduced in the center of B68. This potentially represents evidence for grain coagulation inferred from gas observations. In the literature there are several lines of evidence for grain evolution from dust observations. These include variations in the ratio of visual extinction to reddening, R_V, (Fitzpatrick 2004, and references therein) which have

been attributed to changes in the grain size distribution (Kim et al. 1994; Weingartner & Draine 2001), studies of the far-infrared emission which find a lack of small grains in denser regions (Stepnik et al. 2003), and the requirement for enhanced sub-mm emissivity in star-forming regions (van der Tak et al. 1999; Evans et al. 2001). Theory of grain coagulation suggests significant grain evolution is expected in only a few million years (Weidenschilling & Ruzmaikina 1994), the expected lifetime of the pre-stellar phase (Lee et al. 2001).

To examine what grain evolution (e.g. coagulation) is needed to reach $\delta_d = 0.1$ we have used the MRN (Mathis et al. 1977) grain size distribution. This is given by:

$$dn_{gr} = C n_H a^{-3.5} da, \quad a_{min} < a < a_{max},$$

with $a_{min} = 50$ Å and $a_{max} = 2500$ Å. Draine & Lee (1984) find the normalization for silicate grains to be $C = 10^{-25.11}$ cm$^{2.5}$. Integration of this equation provides $n_{gr} = 1.75 \times 10^{-10} n_H$ for standard ISM grains. To obtain $\delta_d = 0.1$ (while maintaining a$^{-3.5}$) necessitates a minimal change in the size of the smallest grains, to $a_{min} = 150$ Å. This analysis is simplistic as we have not discussed extensions of MRN towards even smaller grains that are needed for the ISM in general (Désert et al. 1990; Weingartner & Draine 2001). However, it is illustrative that only small changes are needed in the lower end of the size distribution to account for the reduction in grain surface area demanded by available gas emission data.

One inconsistency is that we have included small grain photoelectric heating in our models and need to have a warmer central core with less small grains to match NH_3 observations. To this end we investigated the necessity for photo-electric heating in our theory/observation comparison. We find that a reduction of the photoelectric heating rate of more than 50% does not agree with our data (even with a compensating increase in cosmic ray heating).[4] Thus, based upon the adopted formalism for photoelectric heating and dust-gas thermal coupling, we require some small grains to be present in the outer layers but these same grains are absent in the inner core. This is not unreasonable given the large density increase seen in B68 (Fig. 2; Alves et al. 2001).

It is worth noting that Bianchi et al. (2003) find no evidence for dust coagulation based on measurements of the sub-millimeter emissivity and comparison to available grain models. However, the measured value is higher than that of diffuse dust, although only at the 2σ level.

[4]In principle the dust-gas coupling could be stronger at the low density core edges because of warmer dust temperatures and the presence of small grains and weaker in the center due to the lack of small grains. This might further compensate from the loss of very small grains and allow for a greater decrease in photoelectric heating.

5.3. Comparison to Previous Results

A major issue with our suggestion that the UV field is reduced is dust emission models which require a core exposed to ISRF derived by Mathis et al. (1983b), which has $G_0 = 1.6$ (Draine & Li 2001). Moreover the intensity of the ISRF incident on B68 has been estimated independently by Galli et al. (2002) using a variety of dust continuum emission observations with no evidence for any reduction in field strength. Thus there is nearly an order of magnitude difference in UV field strength between gas and dust models.

A likely possibility to reconcile these differences is that there exists an extended layer of diffuse gas around B68 that might unassociated with the core. For instance, Lombardi et al. (2006, in prep.) have used the Near-IR extinction method to map the extinction structure within the Pipe nebula, in which B68 is embedded. This map shows a large degree of extended extinction in this cloud, which provides additional UV shielding for B68. If this layer consists of only 1 mag of extinction, then the strength of the local radiation field for B68 would be increased by a factor of 1/exp(-3) or $G_0 = 2$. Moreover, any H_2 in this layer can contribute to CO self-shielding (Bensch et al. 2003), requiring even less dust extinction. This would allow for higher UV fields in agreement with estimates from the dust emission. We investigated the inclusion of such a halo in our models and find little change to our results for CO isotopologue emission.

5.4. Cloud Support

Lada et al. (2003) used the observed linewidths of $C^{18}O$ and $C^{34}S$ to derive an estimate of the thermal to non-thermal (turbulent) pressure of the B68 core, which is given as:

$$R = \frac{a^2}{\sigma_{nt}^2}$$

In this expression a is the sound speed of the gas and σ_{nt} is the three dimensional velocity dispersion. This measurement used fits to the observed emission profiles that are an integration along the line of sight to demonstrate that B68 is dominated by thermal pressure. In our analysis we have derived a fit to the velocity structure in B68 (Fig. 4) which, for a static model, includes contributions from the thermal and non-thermal velocity dispersions as a function of position in the core.[5]

[5]We note that this analysis includes no contribution from any systematic cloud motions and thus the derived non-thermal contribution is an upper limit.

In Fig. 11 we show how the the thermal to non-thermal pressure ratio varies as a function of radius in B68. There is a sharp variation throughout the object with the center completely dominated by thermal motions and increasing turbulent contributions towards larger radii. At all positions the core is dominated by thermal pressure, confirming the previous result. Lada et al. (2003) derived values of $R \sim 4-5$ for the inner core and $R \sim 1-2$ for the edges. In our model the peak $C^{18}O$ abundance is found at r $\sim$ 0.04 pc, a point which corresponds to $R \sim 5$, close to the value inferred from observation. Thus, in cores with significant abundance and velocity field structure, the line of sight average velocity dispersion from the emission profile is heavily weighted to radii which have the largest abundance.

It is worth noting that B68 is dominated by thermal pressure, but it is not an isothermal object. In our preferred model that matches both CO isotopologues and NH_3 ($\delta_d = 0.1$; § 4.3.2), $> 95\%$ of the enclosed mass lies in layers with a gas temperature variation of ~ 3 K. These changes are within the temperature range examined in the thermal balance and stability study of B68 by Galli et al. (2002). However, the sense of the gradient is opposite to what is normally examined for a pre-stellar object (i.e. the temperature increases inwards). Nonetheless these changes are small and it is likely that the conclusions of Galli et al. (2002) are still relevant and these objects will have similar characteristics to isothermal models.

6. Conclusions

We have combined a multi-molecular and multi-transitional observational study and a thermal/chemical model to examine the line of sight gas temperature structure of the Barnard 68 core. Our primary conclusions are as follows.

(1) The gas temperature is cold $\sim 6-7$ K in the layers traced by ^{13}CO and $C^{18}O$ and is warmer ~ 10 K in the gas deeper within the cloud probed by NH_3. For much of the cloud mass the temperature gradient is small ~ 3 K, but increases towards the center. With significantly more observational constraints than previous work, this represents the best determination of the gas temperature structure in pre-stellar cores.

(2) In agreement with previous studies (Hotzel et al. 2002b; Bergin et al. 2002) we find evidence for large-scale freeze-out of both CO isotopologues and demonstrate that B68 is dominated by thermal pressure.

(3) To match the data to a model we require a UV field that is weaker than the standard IRSF. This is in conflict with a previous examination of the dust emission and we discuss how this discrepancy can be resolved.

(4) We find that the dust-gas coupling rate must be reduced by nearly an order of magnitude, potentially through a lack of small grains in the densest regions. This presents an argument from gas observations for grain coagulation in the central regions of the core.

Our detailed comparison of molecular emission to a PDR model in a low UV environment finds some differences which can be reconciled by assuming that the physics of dust-gas coupling are represented correctly by changing grain properties. Whether these results have general applicability requires more detailed investigations of other sources with well characterized density structure, preferably with high UV fields. Additional improvements would result from more direct modeling of NH_3 emission.

We are grateful to the referee for a thorough and detailed report which improved this paper. This work is supported by the National Science Foundation under Grant No. 0335207. EAB is grateful to discussions with F. Bensch to D. Lis, M. Tafalla, M. Gurwell, and G. Herczeg for various aspects of data calibration and observing.

REFERENCES

Aikawa, Y., Herbst, E., Roberts, H., & Caselli, P. 2005, ApJ, 620, 330

Alves, J. F., Lada, C. J., & Lada, E. A. 2001, Nature, 409, 159

André, P., Ward-Thompson, D., & Barsony, M. 2000, Protostars and Planets IV, 59

Ashby, M. L. N., Bergin, E. A., Plume, R., Carpenter, J. M., Neufeld, D. A., Chin, G., Erickson, N. R., Goldsmith, P. F., Harwit, M., Howe, J. E., Kleiner, S. C., Koch, D. G., Patten, B. M., Schieder, R., Snell, R. L., Stauffer, J. R., Tolls, V., Wang, Z., Winnewisser, G., Zhang, Y. F., & Melnick, G. J. 2000, ApJ, 539, L115

Bensch, F., Leuenhagen, U., Stutzki, J., & Schieder, R. 2003, ApJ, 591, 1013

Bensch, F., Stutzki, J., & Heithausen, A. 2001, A&A, 365, 285

Bergin, E. A., Alves, J., Huard, T., & Lada, C. J. 2002, ApJ, 570, L101

Bergin, E. A., Hartmann, L. W., Raymond, J. C., & Ballesteros-Paredes, J. 2004, ApJ, 612, 921

Bergin, E. A. & Langer, W. D. 1997, ApJ, 486, 316

Bergin, E. A., Langer, W. D., & Goldsmith, P. F. 1995, ApJ, 441, 222

Bergin, E. A., Neufeld, D. A., & Melnick, G. J. 1998, ApJ, 499, 777

Bianchi, S., Gonçalves, J., Albrecht, M., Caselli, P., Chini, R., Galli, D., & Walmsley, M. 2003, A&A, 399, L43

Black, J. H. 1994, in ASP Conf. Ser. 58: The First Symposium on the Infrared Cirrus and Diffuse Interstellar Clouds, 355–+

Boland, W. & de Jong, T. 1982, ApJ, 261, 110

Bonnor, W. B. 1956, MNRAS, 116, 351

Bringa, E. M. & Johnson, R. E. 2004, ApJ, 603, 159

Brown, P. N., Byrne, G. D., & Hindmarsh, A. C. 1989, SIAM J. Sci. Stat. Comput., 10, 1038

Burke, J. R. & Hollenbach, D. J. 1983, ApJ, 265, 223

Collings, M. P., Dever, J. W., Fraser, H. J., & McCoustra, M. R. S. 2003, Ap&SS, 285, 633

Danby, G., Flower, D. R., Valiron, P., Schilke, P., & Walmsley, C. M. 1988, MNRAS, 235, 229

Désert, F.-X., Boulanger, F., & Puget, J. L. 1990, A&A, 237, 215

Dickman, R. L. & Clemens, D. P. 1983, ApJ, 271, 143

Draine, B. T. 1978, ApJS, 36, 595

Draine, B. T. & Lee, H. M. 1984, ApJ, 285, 89

Draine, B. T. & Li, A. 2001, ApJ, 551, 807

Draine, B. T. & Salpeter, E. E. 1979, ApJ, 231, 438

Ebert, R. 1955, Zeitschrift für Astrophysics, 37, 217

Evans, N. J., Rawlings, J. M. C., Shirley, Y. L., & Mundy, L. G. 2001, ApJ, 557, 193

Fitzpatrick, E. L. 2004, in ASP Conf. Ser. 309: Astrophysics of Dust, 33–+

Galli, D., Walmsley, M., & Gonçalves, J. 2002, A&A, 394, 275

Goldsmith, P. F. 2001, ApJ, 557, 736

Habing, H. J. 1968, Bull. Astron. Inst. Netherlands, 19, 421

Hasegawa, T. I. & Herbst, E. 1993, MNRAS, 261, 83

Hogerheijde, M. R. & van der Tak, F. F. S. 2000, A&A, 362, 697

Hotzel, S., Harju, J., & Juvela, M. 2002a, A&A, 395, L5

Hotzel, S., Harju, J., Juvela, M., Mattila, K., & Haikala, L. K. 2002b, A&A, 391, 275

Kim, S.-H., Martin, P. G., & Hendry, P. D. 1994, ApJ, 422, 164

Lada, C. J., Bergin, E. A., Alves, J. F., & Huard, T. L. 2003, ApJ, 586, 286

Lai, S., Velusamy, T., Langer, W. D., & Kuiper, T. B. H. 2003, AJ, 126, 311

Langer, W. D., Graedel, T. E., Frerking, M. A., & Armentrout, P. B. 1984, ApJ, 277, 581

Lee, C. W., Myers, P. C., & Tafalla, M. 2001, ApJS, 136, 703

Leger, A., Jura, M., & Omont, A. 1985, A&A, 144, 147

Mathis, J. S., Mezger, P. G., & Panagia, N. 1983a, A&A, 128, 212

—. 1983b, A&A, 128, 212

Mathis, J. S., Rumpl, W., & Nordsieck, K. H. 1977, ApJ, 217, 425

Neufeld, D. A., Lepp, S., & Melnick, G. J. 1995, ApJS, 100, 132

Sandford, S. A. & Allamandola, L. J. 1988, Icarus, 76, 201

Stepnik, B., Abergel, A., Bernard, J.-P., Boulanger, F., Cambrésy, L., Giard, M., Jones, A. P., Lagache, G., Lamarre, J.-M., Meny, C., Pajot, F., Le Peintre, F., Ristorcelli, I., Serra, G., & Torre, J.-P. 2003, A&A, 398, 551

Tafalla, M., Myers, P. C., Caselli, P., Walmsley, C. M., & Comito, C. 2002, ApJ, 569, 815

Tielens, A. G. G. M. & Hollenbach, D. 1985, ApJ, 291, 722

van Broekhuizen, F. 2005, Ph.D. Thesis

van der Tak, F. F. S., Caselli, P., & Ceccarelli, C. 2005, A&A, 439, 195

van der Tak, F. F. S. & van Dishoeck, E. F. 2000, A&A, 358, L79

van der Tak, F. F. S., van Dishoeck, E. F., Evans, N. J., Bakker, E. J., & Blake, G. A. 1999, ApJ, 522, 991

van Dishoeck, E. F. & Black, J. H. 1988, ApJ, 334, 771

Webber, W. R. 1998, ApJ, 506, 329

Weidenschilling, S. J. & Ruzmaikina, T. V. 1994, ApJ, 430, 713

Weingartner, J. C. & Draine, B. T. 2001, ApJ, 548, 296

Wolfire, M. G., Hollenbach, D., McKee, C. F., Tielens, A. G. G. M., & Bakes, E. L. O. 1995, ApJ, 443, 152

Young, K. E., Lee, J.-E., Evans, N. J., Goldsmith, P. F., & Doty, S. D. 2004, ApJ, 614, 252

Zhou, S., Wu, Y., Evans, N. J., Fuller, G. A., & Myers, P. C. 1989, ApJ, 346, 168

Zucconi, A., Walmsley, C. M., & Galli, D. 2001, A&A, 376, 650

Table 1. Initial Abundances

Species	Abundance[a]
He	0.14
H_2O_{ice}	2.2×10^{-4}
$H_2^{18}O_{ice}$	4.4×10^{-7}
CO	8.5×10^{-5}
^{13}CO	9.5×10^{-7}
$C^{18}O$	1.7×10^{-7}
Fe	3×10^{-8}
Fe^+	1.2×10^{-11}

[a]Abundances are relative to total H.

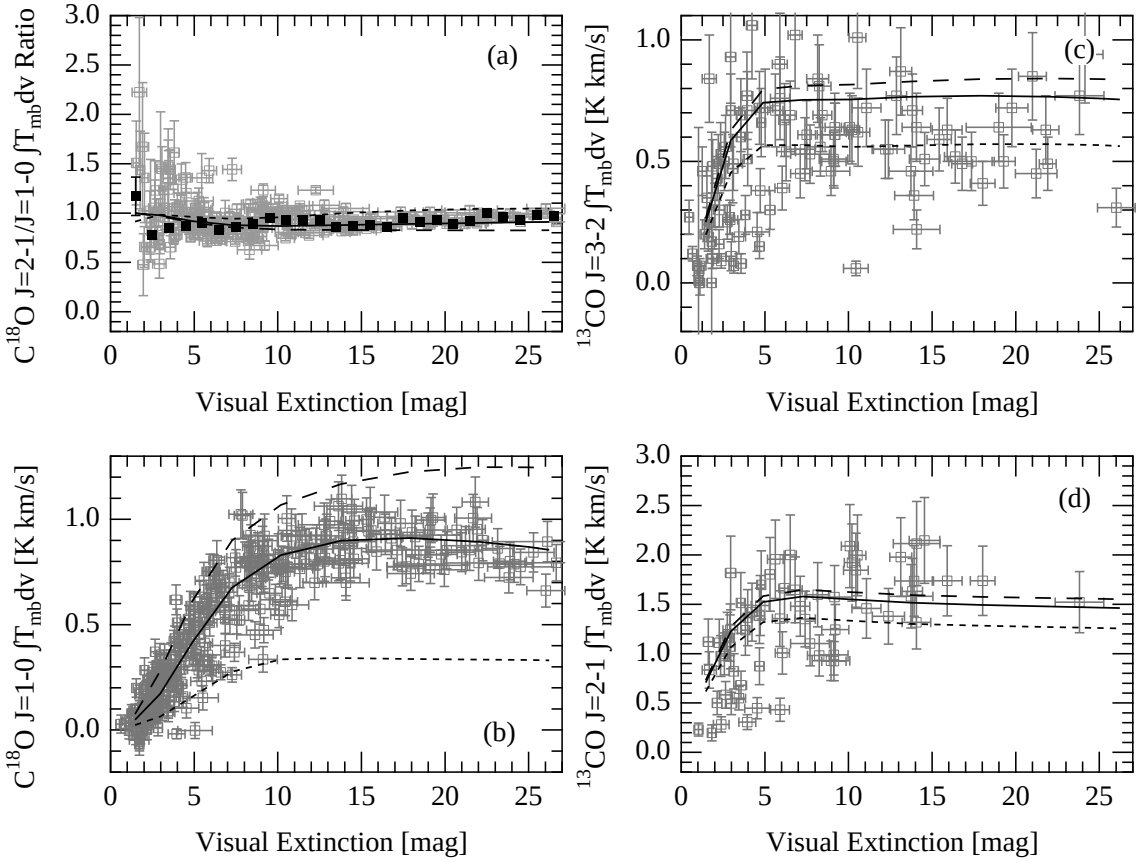

Fig. 1.— Point by point comparison of (a) J= 2 − 1/J= 1 − 0 line ratio, (b) $C^{18}O$ J= 1 − 0 integrated intensity, (c) ^{13}CO J= 2 − 1 integrated intensity and (d) ^{13}CO J= 3 − 2 integrated intensity with A_V for the entire B68 dark cloud. In these plots the data are presented as open squares with error bars while solid curves represent the emission predicted by a model combining chemistry with a Monte-Carlo radiative transfer code. Time dependent model predictions are provided with t = 4×10^4 yr (long dashed line), 1×10^5 yr (solid line), and 3×10^5 yr (short dashed line). In (a) we include 1 mag binned weighted average of the J= 2 − 1/J= 1 − 0 line ratio

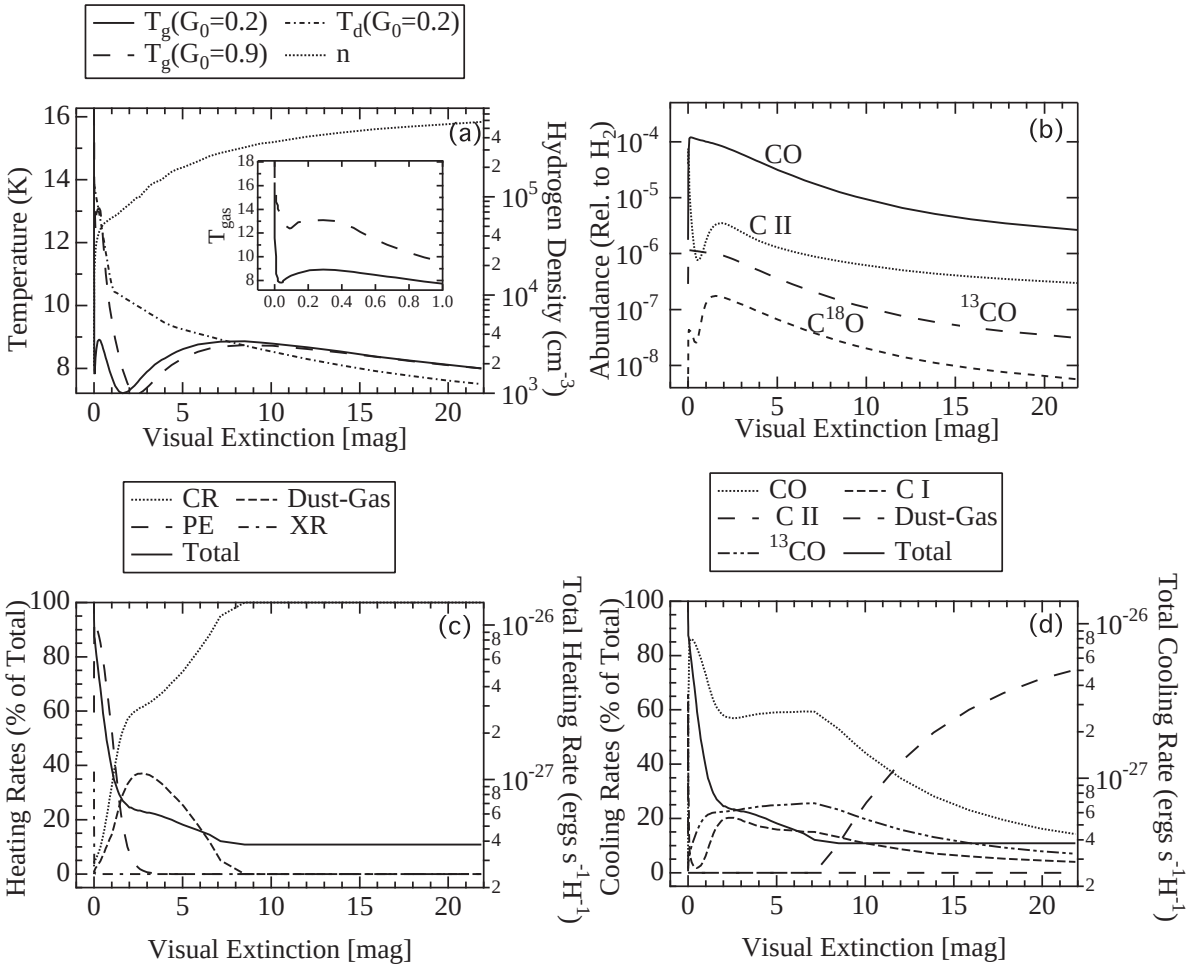

Fig. 2.— Results from a coupled chemical/thermal model of the B68 dark cloud. (a) Gas temperature for two models assuming an external illumination of $G_0 = 0.2$ and 0.9. Dust temperature structure taken from a model of B68 of Zucconi et al. (2001). The gas temperature for the $G_0 = 0.2$ and 0.9 models are identical for $A_V > 2^m$. We do not use a log scale on these figures to emphasize the gas temperature in layers with $A_V > 0.1$ mag, where the molecular lines can be used as probes. (b) Chemical abundances of primary coolants for the $G_0 = 0.2$ model. (c) Primary cooling contributors as percentage of total. Total cooling rate is given as a solid line with axis labeled to right. (d) Primary heating contributors as percentage of total. Total heating rate is given as a solid line with axis labeled to right.

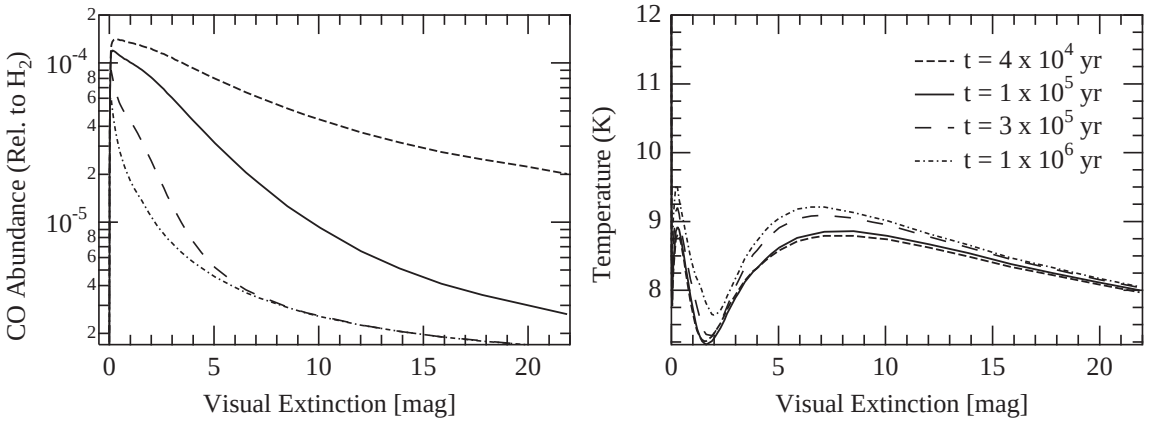

Fig. 3.— *Left:* CO abundance as a function of visual extinction and time. *Right:* Gas temperature as a function of visual extinction and time.

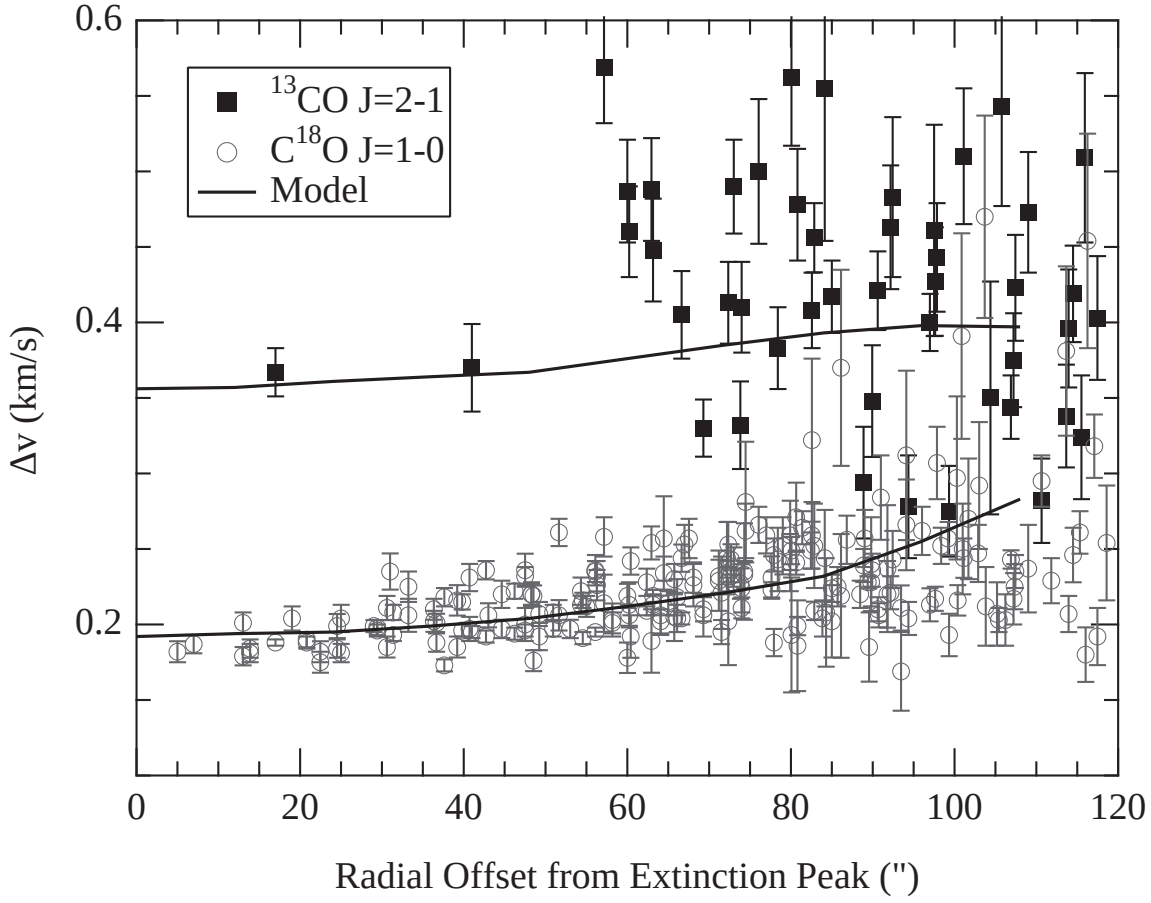

Fig. 4.— Velocity linewidth (FWHM) determined by fitting $C^{18}O$ J=1-0 and ^{13}CO J=2-1 observed and model spectra with Gaussians shown as a function of radial distance from the extinction peak. Data are given as points and model results from the best fit solution as a solid line.

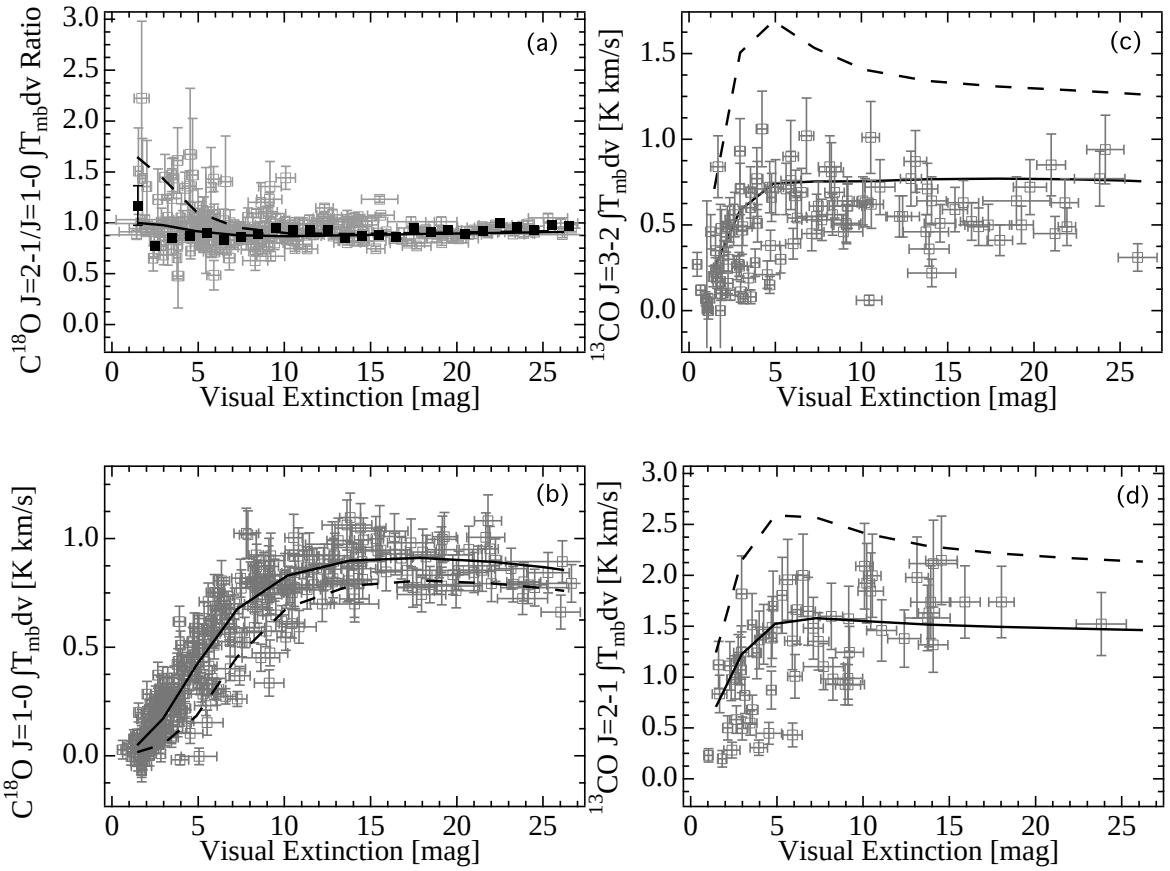

Fig. 5.— Comparison of chemical/thermal models with different values of the radiation field. (a-d) as in Fig. 1. Two values of the external radiation field are examined: $G_0 = 1$ (dashed lines) and $G_0 = 0.2$ (solid lines).

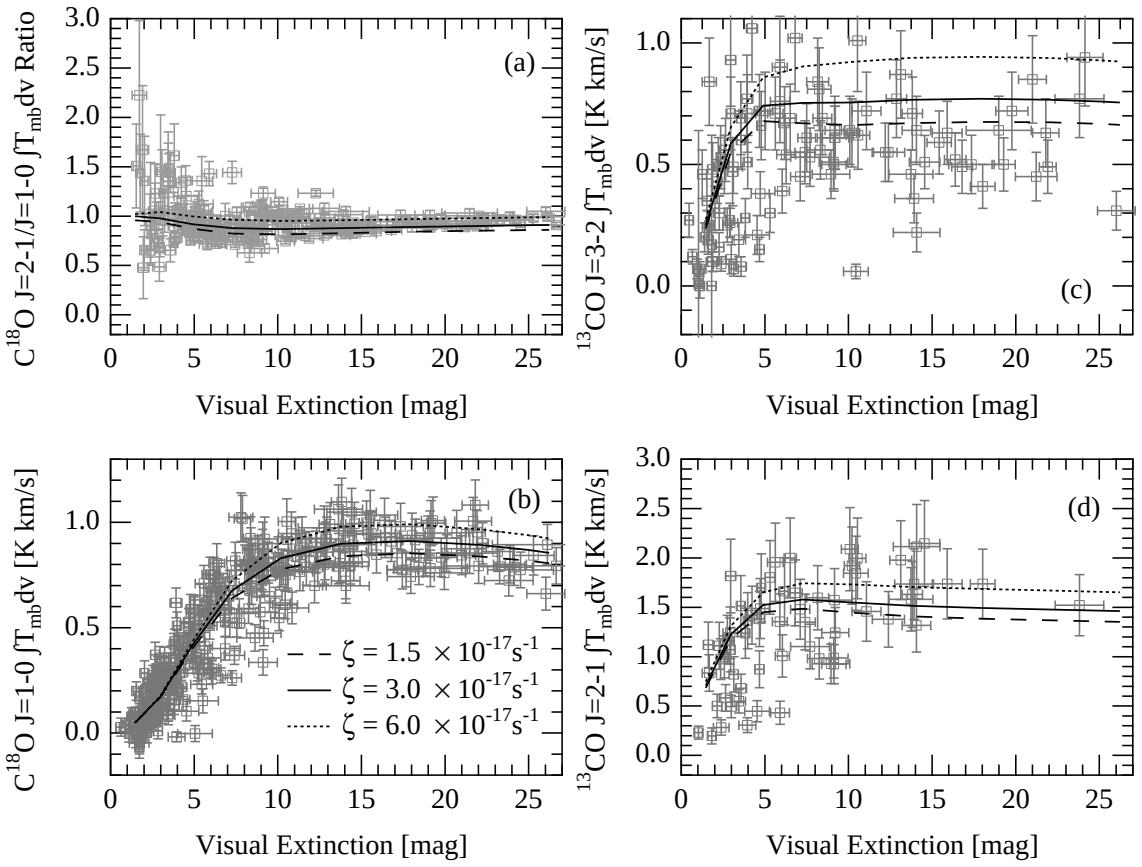

Fig. 6.— Comparison of chemical/thermal models with different values of the cosmic ray ionization rate with labels provided above. (a-d) as in Fig. 1.

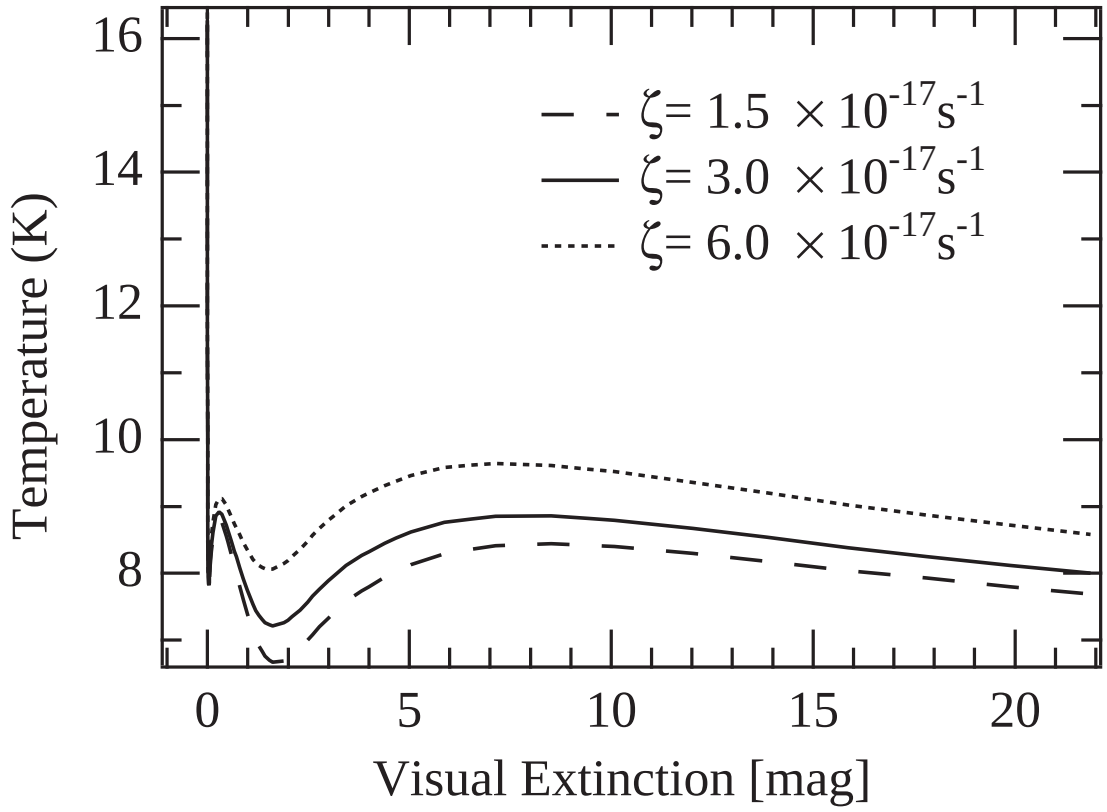

Fig. 7.— Derived temperature structure for models with different values of the cosmic ray ionization rate with labels provided above.

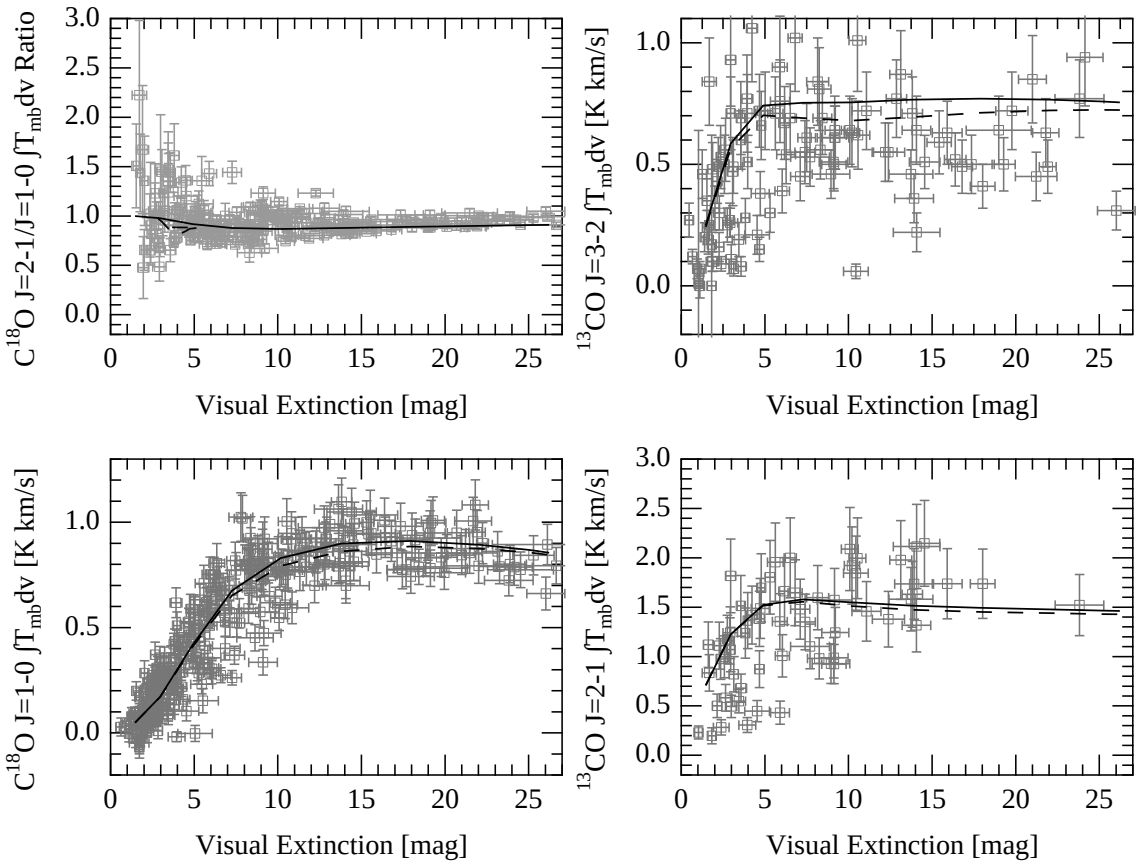

Fig. 8.— Comparison of chemical/thermal models with variable degrees of dust-gas thermal coupling. (a-d) as in Fig. 1. Two values of δ_d are examined: $\delta_d = 1$ (solid line) and $\delta_d = 0.1$ (dashed line).

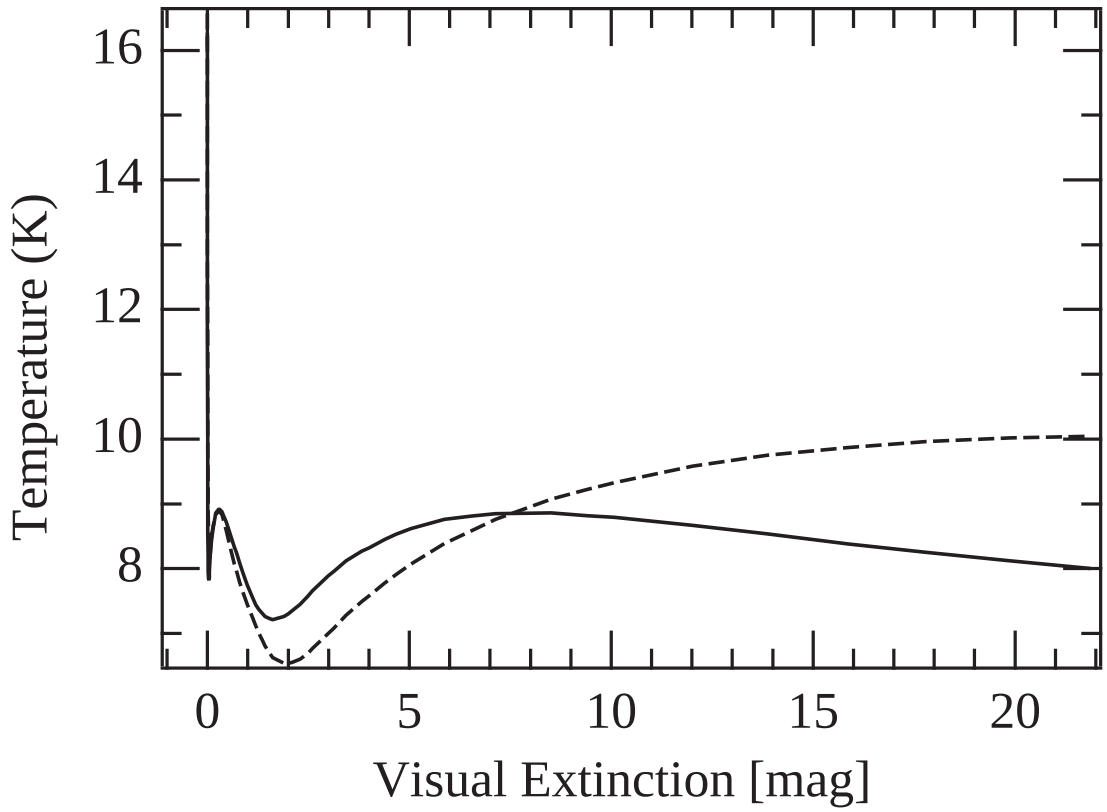

Fig. 9.— Derived temperature structure for models with variable degrees of dust-gas thermal coupling. Two values of δ_d are examined: $\delta_d = 1$ (solid line) and $\delta_d = 0.1$ (dashed line).

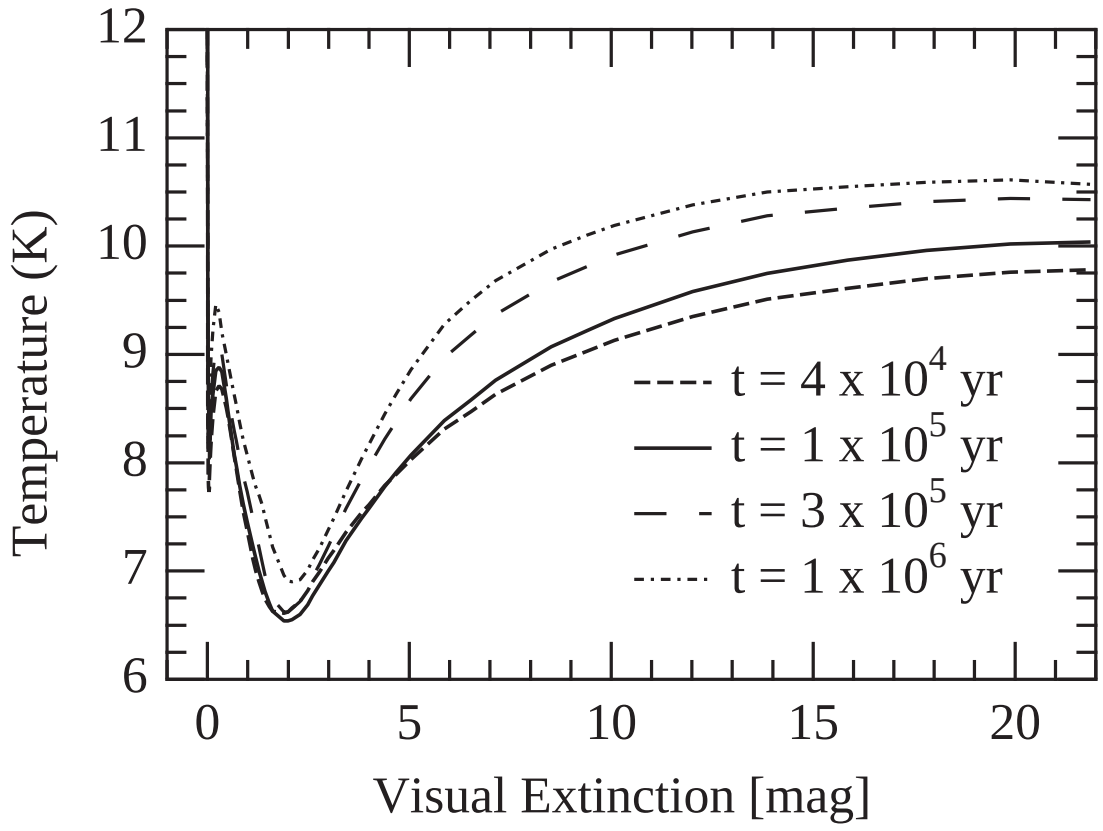

Fig. 10.— Derived temperature structure as a function of time for models assuming $\delta_d = 0.1$.

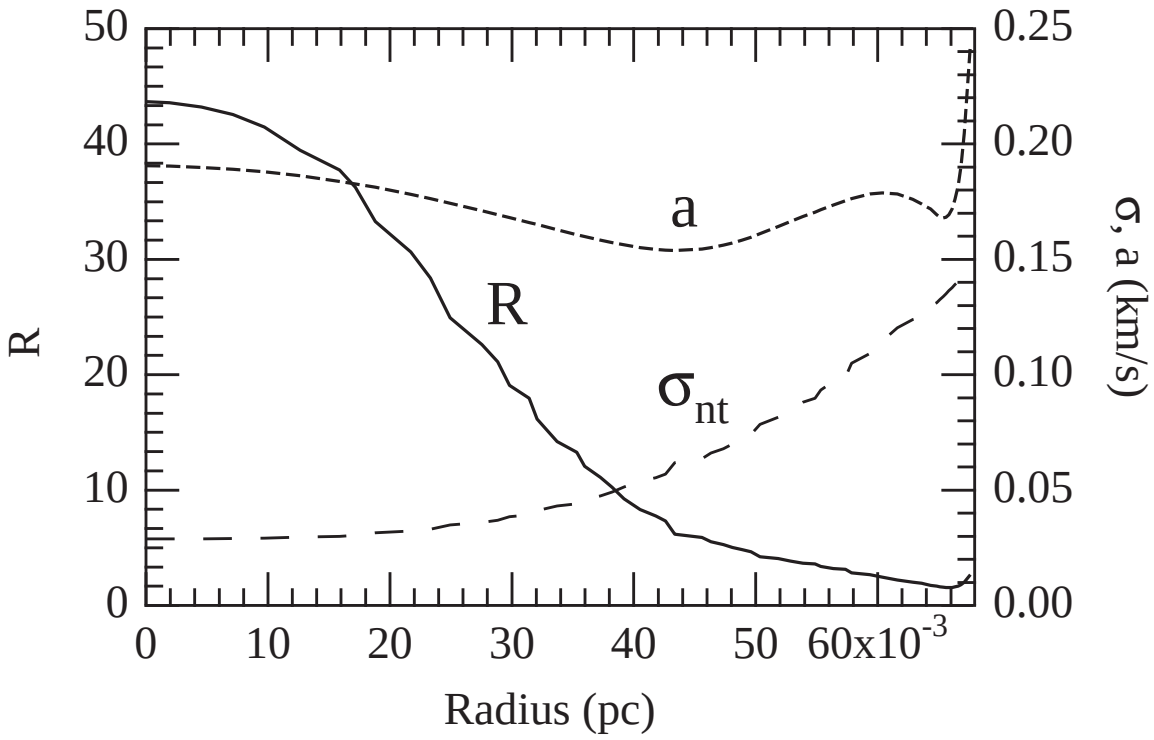

Fig. 11.— Examination of the derived velocity and pressure structure in B68. Left axis shows the value of R, the ratio of thermal to non-thermal pressure, as function of radius. The right axis refers to the values of the thermal (a) and non-thermal (σ_{nt}) velocity dispersion also given as a function of radius.